ChemComm

COMMUNICATION

View Article Online
View Journal | View Issue

Cite this: *Chem. Commun.*, 2023, 59, 9762

Received 27th April 2023,
Accepted 17th July 2023

DOI: 10.1039/d3cc02057f

rsc.li/chemcomm

Sequential chiral induction between organic and inorganic supramolecular helical assemblies for the *in situ* formation of chiral carbon dots†

Piyanan Pranee, [a] Antoine Scalabre, [a] Christine Labrugere,[c] Naoya Ryu, [d] Akira Yano,[e] Nanami Hano, [ah] David Talaga,[b] Yutaka Okazaki, [f] Emilie Pouget, [a] Sylvain Nlate, [a] Sébastien Bonhommeau, [b] Makoto Takafuji, [h] Takehiko Wada, [e] Hirotaka Ihara, [hi] Thierry Buffeteau, [b] Dario M. Bassani *[b] and Reiko Oda *[ag]

Self-organised helical bilayers of dicationic gemini surfactants confined in helical silica nanospace were transformed *in situ* to carbon dots (CDots) *via* pyrolysis. These water-dispersible CDots exhibit electronic absorption spanning the UV and visible range and possess symmetrical circular dichroism (CD) signals, the sign of which depends on the handedness of the helices.

Carbon dots (CDots) are luminescent carbon materials that are less than 10 nm in size and are composed of an amorphous carbon cluster and π-conjugated domains stabilized by surface functional groups.[1,2] CDots have recently attracted much attention for a wide range of applications due to their unique fluorescent properties, good biocompatibility, and easy functionalization.[3,4] It has been previously reported that CDots can be synthesized from various organic compounds by a bottom-up approach through hydrothermal reaction, reflux or pyrolysis.[5,6] The transformation of organic molecules to CDots occurs through the condensation of functional groups, followed by carbonization.[7,8] Meanwhile, chiral CDots with different effects on biological phenomena[9] have shown great potential and promising properties in sensing amino acids, inhibiting peptide assemblies,[10] and enantioselective recognition.[11] For example, cysteine-based L-CDots were effective in glycolysis during the treatment of bladder cancer cells, whereas D-CDots showed no such effects.[12] On the other hand, cysteine and citric acid-based D-CDots were able to enhance root vigor and the enzymatic activity of bean sprouts more effectively than L-CDots.[13] Ma *et al.* found that citric acid- and aspartic acid-based L-CDots worked as strong irreversible inhibitors of tyrosinase (almost 100%), while D-CDots had lower inhibition rates (~30%).[14] Thus, the synthesis and characterization of chiral CDots combining luminescence and chiroptical properties have been at the forefront of designing original optical nanomaterials.

In general, there are three approaches to endow chiroptical properties to CDots: (1) Incomplete carbonization of chiral precursors,[15,16] (2) attaching chiral molecules after the synthesis of the CDots,[17,18] (3) incorporating achiral CDots within chiral supramolecular architectures.[19] For the first method, Deka *et al.* synthesized chiral CDots from different enantiomers of chiral precursors *via* pyrolysis. The CDots obtained presented chiroptical activity originating from the chiral precursor.[15] Meanwhile, Wang *et al.* synthesized chiral CDots by surface modification of achiral carbon cores by D-/L-tryptophan. These CDots showed mirror-image CD spectra resulting from the attached chiral molecules and selectively inhibited the activity of laccase. L-CDots showed a higher inhibition rate than D-CDots under the same reaction condition.[20] Chiral CDots have also been successfully prepared by the co-assembly of achiral CDots with a chiral D-/L-glutamic acid-based supramolecular gelator. The intermolecular bond between CDots and the chiral source induced both CD and Circularly Polarized Luminescence (CPL) activity in the CDots.[19]

Previously, we have reported the self-organisation of an enantiopure tartrate with a gemini-type cationic surfactant, *N*,*N*′-dihexadecyl-*N*,*N*,*N*′,*N*′-tetramethylethylene diammonium (hereafter abbreviated as 16-2-16). 16-2-16 L- or D-tartrate in

[a] *Univ. Bordeaux, CNRS, Bordeaux INP, CBMN, UMR 5248, Pessac F-33600, France. E-mail: reiko.oda@u-bordeaux.fr*
[b] *Univ. Bordeaux, CNRS, Bordeaux INP, ISM UMR 5255, Talence F-33400, France*
[c] *CNRS, Université de Bordeaux, PLACAMAT UMS 3626, Pessac F-33600, France*
[d] *Materials Development Department, Kumamoto Industrial Research Institute, 3-11-38, Higashimachi, Higashi-ku, Kumamoto 862-0901, Japan*
[e] *Institute of Multidisciplinary Research for Advance Materials, Department of Chemistry, Graduate School of Science, Tohoku University, Sendai, 980-8577, Japan*
[f] *Graduate School of Energy Science, Kyoto University, Yoshida-Honmachi, Sakyo-ku, Kyoto 606-8501, Japan*
[g] *WPI-Advanced Institute for Materials Research, Tohoku University, 2-1-1, Katahira, Aoba-Ku, Sendai 980-8577, Japan*
[h] *Department of Applied Chemistry and Biochemistry, Kumamoto University, 2-39-1 Kurokami, Chuo-ku, Kumamoto 860-8555, Japan*
[i] *National Institute of Technology, Okinawa College, Henoko, Nano 905-2192, Japan*

† Electronic supplementary information (ESI) available: Additional information on synthesis and characterization by absorption, fluorescence and Raman spectroscopies, CD, XPS, EA and TEM. See DOI: https://doi.org/10.1039/d3cc02057f

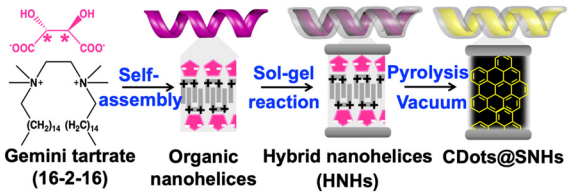

Scheme 1 Illustration of the synthesis of chiral CDots using silica nanohelices.

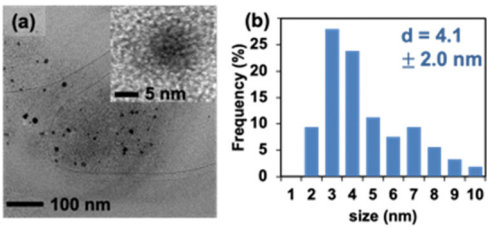

Fig. 2 HR-TEM images (a) and size distribution (b) of CDots.

water self-assembles to form right- or left-handed (RH and LH, respectively) double-bilayer helical structures (Scheme 1).[21] The chiral nanohelices can be used as templates for the sol–gel polycondensation of tetraethyl orthosilicate (TEOS) to obtain silica-organic hybrid nanohelices (HNHs), with 29.4 wt% of 16-2-16 and tartrate content.[22] These HNHs show strong CD signals below 250 nm which originate from the tartrate anions (Fig. 1a).

When the HNHs are pyrolyzed under vacuum at 600 °C for 5 hr, they transform into a black powder (Fig. S1, ESI†) that gives rise to a broad absorption band spanning throughout the UV and visible range, with two strong peaks centred at 223 and 247 nm (Fig. 1(b)). This material also clearly shows chiroptical properties as evidenced by symmetric CD spectra in the 200–700 nm wavelength range with a negative signal for the LH helices and a positive signal for the RH helices. The CD signal above 250 nm indicates the formation of a new structure after pyrolysis with an asymmetry factor (g_{abs}) of -3.0×10^{-4} (LH) and 3.0×10^{-4} (RH) at 570 nm, as calculated from $g_{abs} = \Delta\varepsilon/\varepsilon = \theta(\text{mdeg})/(32\,980\ A)$ where θ = ellipticity, A = absorbance, $\Delta\varepsilon$ = molar circular dichroism. This signal is very different from that of the HNHs. The transmission electron microscope (TEM) images did not show significant morphology modification of the silica helices before and after pyrolysis (Fig. 1(c) and (d)). The double-bilayer organic structure was thus *in situ* converted to CDots while confined inside the helical silica framework. To further confirm the *in situ* transformation, the silica framework was removed by dissolving it in 6 M NaOH at 60 °C and washing with water. High-resolution TEM (HR-TEM) images (Fig. 2) of the resulting solution confirm the presence of nanoparticles with an average size of 4.1 ± 2.0 nm. The selected area electron diffraction (SAED) observation confirmed the presence of graphitic structure (Fig S2, ESI†). From these results, we conclude that pyrolysis of the HNHs leads to the formation of CDots which are confined inside the silica helices (CDots@SNHs) (Scheme 1). The CDots without silica nanotemplate showed no CD signal while they retained similar absorbance signals. The origin of the chiroptical signal of these CDots is thus due to their chiral organization inside the chiral nanospace of the silica structure.

In order to investigate if such CD signals originate from the incomplete pyrolysis of tartrate, a control experiment was carried out by pyrolyzing a sample of 16-2-16 gemini tartrate under the same conditions as above but without the helical silica template. Blue-emitting CDots were obtained after pyrolysis, but no CD signals were detected (Fig. S3, ESI†).

No visible chiral mesostructures remained from the carbonization of the gemini tartrate. These results indicate that the silica nanohelices are necessary for the induction of the chiroptical properties in the CDots.

The elemental contents of HNHs before and after pyrolysis were characterized using elemental analysis (EA, Table S1, ESI†). HNHs (before pyrolysis) contained C (20.9%), N (1.1%), and H (4.4%) with an N/C ratio of 0.05. This ratio corresponds to the composition of the gemini tartrate. The elemental contents of C, N, and H of CDots@SNHs was found to be 8.12%, 0.27%, and 0.65%, respectively, with an N/C ratio of 0.03. This shows that the organic content decreased significantly during pyrolysis with a higher loss of N compared to C.[23] The decrease in N/C contents during the pyrolysis is due to their transformation into volatile molecules (NOx species), NH_3, HCN and N_2[24,25] whereas from the C contents, they transformed in majority to CDots with some transformation to CO_2 gas.

X-ray photoelectron spectroscopy (XPS) was used to investigate the chemical compositions and structure of the CDots@SNHs. The spectra show four predominant peaks corresponding to 9.24% carbon (C1s), 0.21% nitrogen (N1s), 57.53% of oxygen (O1s), and 32.66% Si (Si2p) (Fig. 3(a) and (b)). As shown in Fig. 3(c), the deconvolution of the high-resolution analysis of the C1s peak indicates contributions at 283.8 eV (58.34%) assigned to sp^2 graphitic structures in CDots@SNHs,

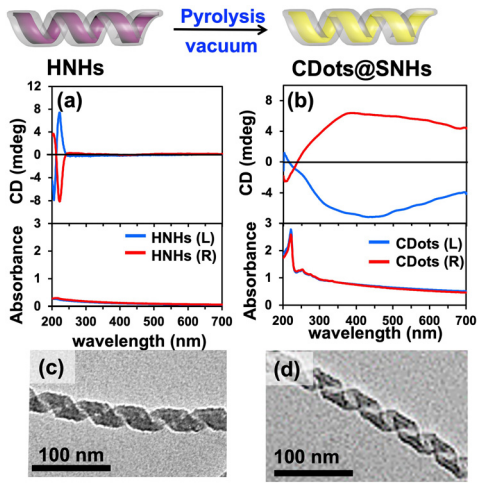

Fig. 1 CD and absorption spectra of (a) LH/RH-HNHs and (b) CDots@LH/RH-SNHs in water. TEM images of (c) LH-HNHs and (d) CDots@LH-SNHs.

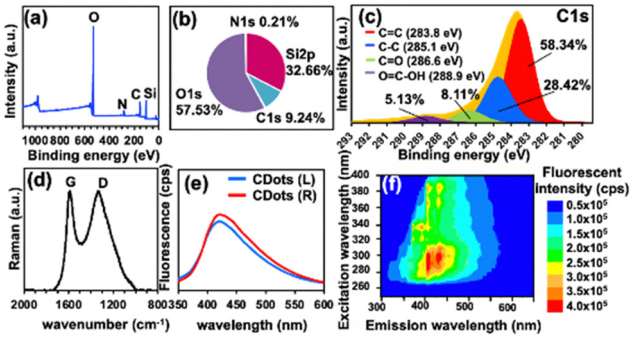

Fig. 3 XPS spectrum (a), elemental contents (b), HR-XPS of C1s (c) and Raman spectrum (d) with the 633 nm excitation wavelength of chiral CDots@SNHs. The fluorescence spectra, $\lambda_{ex\ 290}$, (e) and 2D fluorescence spectra (f) of CDots@LH-SNHs in DMF.

along with peaks at 285.1 eV (28.42%), 286.6 eV (8.11%), 288.9 eV (5.13%) corresponding to C–C, C═O and O═C–OH bonds, respectively. The Raman spectrum recorded using 633 nm excitation (Fig. 3(d)) shows two broad D and G bands at ∼1330 and ∼1590 cm^{-1}, respectively. The G band is related to the E_{2g} mode of graphite and the vibration of sp^2-bond carbon atoms in hexagonal lattices, whereas the D band originates from the vibrations of carbon atoms in disordered graphite. Therefore, both Raman and XPS data confirm that the CDots are principally composed of sp^2 and sp^3 carbon atoms.[26,27] The I_D/I_G ratio of chiral CDots which provides the disorder and crystallite size of graphitic layers in CDots was ∼1.[28] The Raman spectrum is very similar to the one observed for graphene oxide materials.[29]

The 2D fluorescence spectra of CDots@SNHs dispersed in H_2O are shown in Fig. S4 (ESI†). The excitation-dependent emission intensity and wavelength are typical of CDots.[30] As for the chiral CDots@SNHs in H_2O, a maximum emission at 352 nm could be observed under an excitation wavelength of 270 nm. The photoluminescence property of SNHs@CDots was strongly affected by the dispersion medium.[31] Indeed, the emission peak of CDots@SNHs in dimethylformamide (DMF) was red-shifted to 425 nm (Fig. 3(e), (f), and Fig. S5, ESI†). The shift in fluorescence emission of CDots@SNHs may be related to the effect of medium polarity and/or to H-bonding with surface functional groups on the CDots.[32] The stability of CDots@SNHs was studied in water and DMF. While the fluorescence intensity of CDots@SNHs in DMF remained stable, that in water decreased dramatically over 5 days (Fig. S6, ESI†) even though the CD spectra and absorbance in water did not change during this time (Fig. S7, ESI†). Although dynamic quenching of CDot emission by water has been speculated,[33] the slow loss of emission upon addition of water is incompatible with an excited-state process. Therefore, we assign this to the formation of non-emissive trap states.

Finally, to completely exclude that the chiroptical properties result from the chirality of the tartrate starting material, we exchanged the tartrate anion with achiral azide (N_3^-) anions inside the HNHs before pyrolysis as reported previously (Fig. S8, ESI†).[22,34] The azide ion was selected since it does not interfere with the CD signal by absorbing in the UV-visible spectral region. Thus, the loss of the CD signal in the UV-visible region confirms the complete exchange of tartrate by azide (Fig. S9, ESI†). After pyrolysis at 600 °C, the azide(N)-doped CDots@SNHs showed strong and mirror image CD signals (Fig. S10(a), ESI†), indicating that the chiroptical properties of the CDots are a result of chiral induction by the nanohelices and not from the chiral tartrate ions. Following the replacement of tartrate by azide anion, the proportion of N and C of the CDots with respect to Si obtained by HR-XPS after pyrolysis (Fig. S11 and S12, ESI†) was higher than that of tartrate-based CDot@SNHs (1.2% and 60% *vs.* 0.6% and 28% for N and C, respectively). N-doped CDots showed a blue-shift emission at ∼417 nm compared to CDots in Fig. S13 (ESI†). We then investigated whether the chiral induction is specific to the gemini or can be extended to a system in which achiral aromatic monomers are polymerized *in situ* inside HNHs prior to pyrolysis. To this end, 2, 6-dihydroxy naphthalene (DHN) was introduced into the HNHs by ion exchange, followed by polymerization using 1,3, 5-trimethyl-1,3,5-triazinane (TMTA) (Fig. 4).[35,36] In addition to being compatible with the HNHs, this polymer was previously shown to be a promising precursor for nitrogen-rich carbon material. Following ion exchange from tartrate to DHN, the HNHs were pinkish and showed an absorption maximum at 228 nm (Fig. 4(a)) with a ratio of DHN:gemini-CI_2^- (1 : 1). Surprisingly, the DHN-doped HNHs did not show CD signals initially. However, after 3 days at 4 °C, we observed the progressive increase of mirror image CD signals, which possibly originate from the self-organization of DHN inside the HNHs. The colour of HNHs gradually turned purple.

The *in situ* polymerization of DHN in HNHs was induced by addition of 1 equivalent of TMTA to the suspension which was kept at 4 °C for 12 hr. During this time, polymerization was accompanied by a colour change from purple to brown. After that, the excess TMTA was washed away with cold water, and the morphology of polymer-doped HNHs was characterized using TEM (Fig. S14, ESI†), confirming that the helical silica

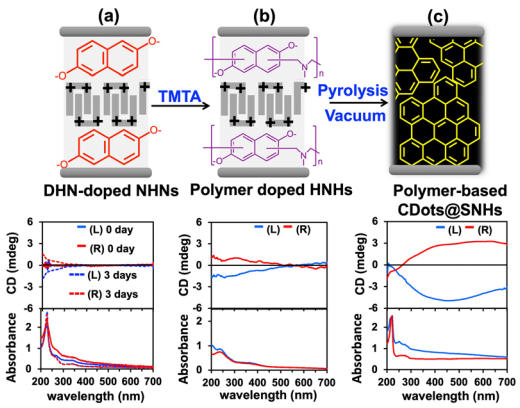

Fig. 4 The illustration of polymerization of DHN in HNHs. CD and absorption spectra of (a) DHN-doped HNHs, (b) polymer-doped HNHs, and (c) polymer-based CDots@SNHs.

framework was unchanged after polymerization. The formation of the polymer was accompanied by an important modification in the absorbance which extended to >600 nm following polymerization.[35] After polymerization, the CD signal of HNHs increased significantly compared to the DHN-doped HNHs (Fig. 4b). These observations suggest that the polymerization enhances the chiroptical properties of the system. However, fluorescence from DHN-doped HNHs and polymer-doped HNHs was not clearly observed due to its low intensity (Fig. S15, ESI†).

The polymer-doped HNHs were subsequently pyrolyzed to afford a black powder exhibiting mirror image CD signals similar to CDots@SNHs. The I_D/I_G ratio calculated from the integrated intensities of D and G Raman bands is ~0.94. Along with the decrease in this value, the presence of a sharp and well-defined peak at 1590 cm^{-1} indicates that CDots@SNHs prepared from the DHN/TMTA polymer have a higher graphitic carbon content (Fig. S16, ESI†). The CD and absorbance signals of the three CDots@SNHs systems are compared in Fig. S10 (ESI†). They are all relatively similar and characterized by a progressive decrease in absorbance which spans from 200 nm to 700 nm spectral range. In addition, the CD signals were negative (positive) below 320 nm and switch signs to positive (negative) broad bands for the right (left) handed helices. Exchanging the counterions to achiral ones did not suppress the induced chirality in the final CDots systems. We have demonstrated the *in situ* formation of chiral CDots synthesized within the nanometric confinement of a helical silica framework. These represent the first examples of CDots showing CD signals in the entire UV-Vis wavelength range extending from 200 nm to 700 nm.

Importantly, we show that the chirality of a helical silica template was the origin of the chirality of the CDots. This represents a unique example in which a chiral organic molecule is used to template the formation of a helical inorganic object, which is in turn used to induce chirality in CDots prepared from organic guests. These results thus demonstrate the high potential for chiral induction from mesoscopic chiral frameworks to carbon-based nanoparticles.

This work was supported by the CNRS and Université de Bordeaux. We thank the financial support from the ANR-21-CE09-0012-01 and the expertise of Placamat platform UAR3626.

Conflicts of interest

There are no conflicts to declare.

Notes and references

1 V. Georgakilas, J. A. Perman, J. Tucek and R. Zboril, *Chem. Rev.*, 2015, **115**, 4744–4822.
2 I. Papagiannouli, M. Patanen, V. Blanchet, J. D. Bozek, M. de Anda Villa, M. Huttula, E. Kokkonen, E. Lamour, E. Mevel, E. Pelimanni, A. Scalabre, M. Trassinelli, D. M. Bassani, A. Lévy and J. Gaudin, *J. Phys. Chem. C*, 2018, **122**, 14889–14897.
3 J. Liu, R. Li and B. Yang, *ACS Cent. Sci.*, 2020, **6**, 2179–2195.
4 Y. Yan, J. Gong, J. Chen, Z. Zeng, W. Huang, K. Pu, J. Liu and P. Chen, *Adv. Mater.*, 2019, **31**, 1808283.
5 M. Otten, M. Hildebrandt, R. Kühnemuth and M. Karg, *Langmuir*, 2022, **38**, 6148–6157.
6 K. Yin, D. Lu, L. Wang, Q. Zhang, J. Hao, G. Li and H. Li, *J. Phys. Chem. C*, 2019, **123**, 22447–22456.
7 X. Li, S. Zhang, S. A. Kulinich, Y. Liu and H. Zeng, *Sci. Rep.*, 2014, **4**, 4976.
8 Y. Zhou, S. K. Sharma, Z. Peng and R. M. Leblanc, *Polymers*, 2017, **9**, 67.
9 H. Yan, M. Cacioppo, S. Megahed, F. Arcudi, L. Đorđević, D. Zhu, F. Schulz, M. Prato, W. J. Parak and N. Feliu, *Nat. Commun.*, 2021, **12**, 7208.
10 E. Arad, S. K. Bhunia, J. Jopp, S. Kolusheva, H. Rapaport and R. Jelinek, *Adv. Ther.*, 2018, **1**, 1800006.
11 Y. Zhang, L. Hu, Y. Sun, C. Zhu, R. Li, N. Liu, H. Huang, Y. Liu, C. Huang and Z. Kang, *RSC Adv.*, 2016, **6**, 59956–59960.
12 F. Li, Y. Li, X. Yang, X. Han, Y. Jiao, T. Wei, D. Yang, H. Xu and G. Nie, *Angew. Chem., Int. Ed.*, 2018, **57**, 2377–2382.
13 M. Zhang, L. Hu, H. Wang, Y. Song, Y. Liu, H. Li, M. Shao, H. Huang and Z. Kang, *Nanoscale*, 2018, **10**, 12734–12742.
14 Y. Ma, M. Zhang, Z. Deng, X. Wang, H. Huang, K. Yang, B. Yuan, Y. Liu and Z. Kang, *Nanoscale*, 2022, **14**, 1202–1210.
15 M. J. Deka and D. Chowdhury, *RSC Adv.*, 2017, **7**, 53057–53063.
16 L. Đorđević, F. Arcudi, A. D'Urso, M. Cacioppo, N. Micali, T. Bürgi, R. Purrello and M. Prato, *Nat. Commun.*, 2018, **9**, 3442.
17 N. Suzuki, Y. Wang, P. Elvati, Z.-B. Qu, K. Kim, S. Jiang, E. Baumeister, J. Lee, B. Yeom, J. H. Bahng, J. Lee, A. Violi and N. A. Kotov, *ACS Nano*, 2016, **10**, 1744–1755.
18 M. Vázquez-Nakagawa, L. Rodríguez-Pérez, M. A. Herranz and N. Martín, *Chem. Commun.*, 2016, **52**, 665–668.
19 A. Li, D. Zheng, M. Zhang, B. Wu and L. Zhu, *Langmuir*, 2020, **36**, 8965–8970.
20 X. Wang, M. Zhang, Y. Ma, J. Wu, Y. Wang, H. Huang, Y. Liu and Z. Kang, *Appl. Surf. Sci.*, 2022, **583**, 152540.
21 R. Oda, S. J. Candau and I. Huc, *Chem. Commun.*, 1997, 2105–2106.
22 Y. Okazaki, N. Ryu, T. Buffeteau, S. Pathan, S. Nagaoka, E. Pouget, S. Nlate, H. Ihara and R. Oda, *Chem. Commun.*, 2018, **54**, 10244–10247.
23 W.-J. Liu, W.-W. Li, H. Jiang and H.-Q. Yu, *Chem. Rev.*, 2017, **117**, 6367–6398.
24 H. Nan, Z. Xiao, L. Zhao, F. Yang, H. Xu, X. Xu and H. Qiu, *ACS Sustainable Chem. Eng.*, 2020, **8**, 12197–12207.
25 C.-Z. Li and L. Tan, *Fuel*, 2000, **79**, 1899–1906.
26 X. Zhang, J. Gu, A. Pang and J. Yang, *Nanotechnology*, 2016, **27**, 165704.
27 I. M. Ferrer, J. C. Vinci, N. W. Guterry, V. M. Colón, J. F. Destino, F. V. Bright and L. A. Colón, *Appl. Spectrosc.*, 2015, **69**, 1082–1090.
28 V. Lee, L. Whittaker, C. Jaye, K. M. Baroudi, D. A. Fischer and S. Banerjee, *Chem. Mater.*, 2009, **21**, 3905–3916.
29 M. Yoshikawa, M. Murakami and Y. Fujita, *J. Raman Spectrosc.*, 2022, **53**, 1394–1401.
30 Z. Ramezani, M. Qorbanpour and N. Rahbar, *Colloids Surf., A*, 2018, **549**, 58–66.
31 D. Chao, W. Lyu, Y. Liu, L. Zhou, Q. Zhang, R. Deng and H. Zhang, *J. Mater. Chem. C*, 2018, **6**, 7527–7532.
32 P. Mohammad-Jafarieh, A. Akbarzadeh, R. Salamat-Ahangari, M. Pourhassan-Moghaddam and K. Jamshidi-Ghaleh, *BMC Chem.*, 2021, **15**, 53.
33 J. Wei, Y. Yuan, H. Li, D. Hao, C. Sun, G. Zheng and R. Wang, *New J. Chem.*, 2018, **42**, 18787–18793.
34 A. Scalabre, Y. Okazaki, B. Kuppan, T. Buffeteau, F. Caroleo, G. Magna, D. Monti, R. Paolesse, M. Stefanelli, S. Nlate, E. Pouget, H. Ihara, D. M. Bassani and R. Oda, *Chirality*, 2021, **33**, 494–505.
35 M. N. Khan, Y. Orimoto and H. Ihara, *Chem. Commun.*, 2018, **54**, 13204–13207.
36 H. Noguchi, M. Sultana, N. Hano, Y. Kuwahara, M. Takafuji, S. Nagaoka, H. Qiu and H. Ihara, *J. Nanomater.*, 2020, **10**, 1882.